Numerical Methods in Civil Engineering

Influence of Dilation Angle of Soil on Seismic Displacements of Gravity Retaining Walls using Upper Bound Limit Analysis Method

Peiman Sharifi*, Orang Farzaneh, Faradjollah Askari*****

ARTICLE INFO

Article history:
Received:
April 2020.
Revised:
May 2020.
Accepted:
May 2020.

Keywords:
Seismic Displacement, Dilation Angle, Gravity Retaining Wall, Yield Acceleration, Performance

Abstract:

In this paper, permanent displacements of gravity retaining walls with back and front fill under seismic excitation due to sliding is investigated. In this regard, by using the upper bound theorem of limit analysis, an expression is presented for obtaining the yield acceleration coefficient and also, critical angles of failure wedges are calculated. Several comparisons are made with other solutions in literature. Effect of variation of dilation angle and ratio of the height of front fill to backfill soil is evaluated on seismic performance of a gravity retaining wall. Results showed that by increasing dilation angles from zero to internal friction angle of the soil, the values of seismic displacement inclines.

1. Introduction

Due to the unprecedented attention of engineering society to the performance of structures under seismic loading in the recent decade, the displacement-based analysis of structures during an earthquake is extremely in demand to improve seismic designing principles and to better predict possible failures and damages. Since Iran experiences a considerable number of destructive earthquakes each year, the seismic stability of structures is profoundly investigated. One of the key geotechnical structures which play a critical role in protecting other structures from possible failures is gravity retaining wall. As a result, understanding their performance and behaviour during an earthquake is highly recommended. Geotechnical authors have been attempting to propose the most accurate and yet the simplest way possible to evaluate gravity retaining walls' behaviour under seismic loads. Until around 1960s, using pseudo-static factor of safety was the most frequent method in seismic stability analysis.

** Corresponding Author: Graduated Student, Department of Civil Engineering, University of Tehran, Tehran, Iran, Email: P.sharifi@ut.ac.ir*
*** Associate Professor, Department of Civil Engineering, Faculty, University of Tehran, Tehran, Iran.*
**** Associate Professor, Geotechnical Engineering Research Center, International Institute of Earthquake Engineering and Seismology (IIEES), Tehran, Iran.*

In the 60s, Newmark [1] developed sliding block method which despite its simplicity, brought a useful criterion to assess seismic performance of slopes. He proposed that by considering the pseudo-static factor of safety equal to 1, horizontal seismic acceleration coefficient (k_h) is actually yield acceleration coefficient (k_y). Double time integration of the difference between yield acceleration and actual earthquake acceleration results in permanent seismic displacement, i.e., whenever the system acceleration exceeds the yield acceleration, the whole structure starts to move. Newmark's procedure was an inspiration for other authors to push back the borders of its application. In 1979, Richards and Elms [2] expanded Newmark's method for retaining walls. Subsequently, several authors initiated numeric analyses to address retaining walls seismic displacement under various situations [3,4]. Whitman and Liao [5] used more simplifications on assumptions adapted by Richards and Elms. In recent years, many approaches have been proposed to investigate the seismic behaviour of the retaining wall under various conditions; Deyanova et al [6] performed non-linear time-history analyses of gravity earth-retaining walls and compared the results with Newmark-based methods and provided recommendations for preliminary seismic design of gravity walls. Taravati and

Ardakani [7] studied the seismic behaviour of gravity retaining wall built near a rock face.
Fathipour et al [8] studied the active and passive earth pressures on the retaining structures having an unsaturated backfill.
Other authors who studied the behaviour of associative and non-associative material and their effect on the behaviour of common geotechnical structures; i.e., Davis [9], Chen [10], Michalowski and Mróz [11], Drescher and Detournay [12], and Veiskarami et al [13].
However, in 2007, Michalowski [14] proposed a new formulation based on upper bound theorem of limit analysis to calculate the permanent displacements of slopes. To do so, a multi-block mechanism was considered. By using velocity and acceleration hodograph, he studied blocks interactions toward each other. He mentioned that assuming the deformation of the material to be in the borders of associated flow rule with a convex yield condition, the upper and lower bound theorems are both applicable in the analyses. However, when tracking the finite displacements of a structure, the associated flow rule may lead to progressively inaccurate displacements, as the granular soils exhibit dilation that is typically less than that predicted by the associative law [14].
Consequently, in order to calculate displacement of gravity retaining walls with back and front fill under seismic loading, the current paper suggests an approach based on the method proposed by Michalowski involving associated and non-associated flow of soils. It also investigates the effect of dilation angle on seismic displacement of gravity retaining wall.

2. Methodology

In the current paper, based on upper bound theorem of limit analysis, a series of formulations are going to be proposed to generate yield acceleration coefficient. Consequently, seismic displacement of gravity retaining walls will be calculated using Newmark's sliding block. The procedure concentrates on a three-wedge soil-wall system which provides pieces of evidence for the front fill effect on the amount of displacement the system experiences during earthquake excitation. The following assumptions are used in proposing formulations:

- The front and backfill and also the wall itself are solid.
- The failure surface is interpreted here as a shear band.
- The soil is dry.

Initiation of plastic deformation coincides with equality of stress state and yield condition of structure [14]. If the result of this condition forms a convex yield surface in the stress space, and the deformation is governed by the normality (or associative) flow rule, it can be concluded that in any kinematically admissible failure mechanism, the rate of internal work is not less than the rate of true external forces [15].

$$\int_V \sigma_{ij}^k \dot{\varepsilon}_{ij}^k dV \geq \int_S T_i v_i dS + \int_V X_i v_i^k dV \qquad (1)$$

The integral over entire volume V on the left side of Eq. (1) represents energy dissipated in the entire mechanism which is called the rate of internal work. Integral over entire boundary S on the right side shows the external work rate of surface load T_i on S, which has got deformation velocity of v_i (kinematic boundary condition). The external work rate of distributed forces X_i per unit volume (such as weight, and inertial) in the kinematically admissible velocity field v_i^k is given by the latter integral in Eq. (1). Associated stress field σ_{ij} marked with superscript k is compatible with the selected mechanism [12]. $\dot{\varepsilon}_{ij}$ is the strain rate compatible with real or virtual displacement rate v_i or v_i^k [10].
The system in Fig. 1 comprises three wedges. A soil mass with the height of H_1, which covers the height of wall, having an internal friction angle φ_1 and unit weight γ_1, is taken as the first wedge. Correspondingly, a soil mass with the height of H_2, having internal friction angle φ_2 and unit weight γ_2, is considered as the second wedge. The wall itself is assumed as the third wedge with unit weight γ_3 which is as high as the first wedge. δ_1, δ_2, and δ_3 are interface friction angles of the wall with backfill soil, the front soil, and the soil at the base, respectively. Horizontal and vertical seismic coefficients k_h and k_v are applied to the whole soil-wall system to represent seismic forces. Two parallel lines in Fig. 1 shows a thin layer of soil indicating a failure surface.

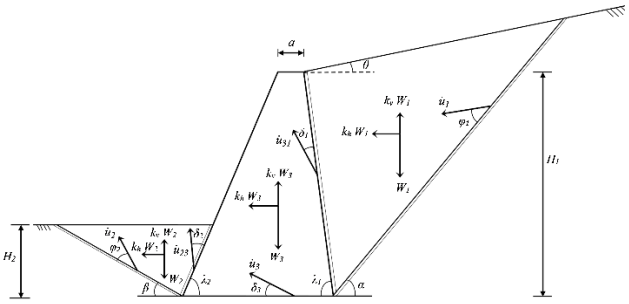

Fig. 1: Soil-wall system's failure mechanism

Based on associated flow rule, velocity vectors of wedges make certain angles with failure surface in kinematic boundary conditions [16]. These angles for the first and the second wedges with their corresponding soil failure surfaces are φ_1 and φ_2; and with their corresponding failure surfaces of soil-wall are δ_1 and δ_2, respectively. The angle between velocity vector and the base is δ_3. As it is shown in Fig. 2, $\dot{u}_1$, $\dot{u}_2$, and $\dot{u}_3$ are the velocities of the first, second, and the third wedges; and $\dot{u}_{31}$ and $\dot{u}_{23}$ are relative velocities between the wall and the first and second wedges, respectively. Except for $\dot{u}_3$ which has got a certain alignment with a horizontal line, the angles of other velocity vectors with a horizontal line, set various shapes for velocity hodograph.

The angle between velocity vectors of wedges (not the relative ones) and the corresponding shear band must be introduced to address the velocity vectors. The velocity hodograph forms by comparison of these angles. In Fig. 2, all the possible alignments of velocity vectors of the wedges are shown. Based on $\dot{u}_1$ and $\dot{u}_3$ comparison of three cases in Fig. 2(a)(b)(c), $\dot{u}_2$ and $\dot{u}_3$ comparison of two cases in Fig. 2(d)(e), and in total, 6 cases of hodograph are going to be introduced. Fig. 2(f), gives an example of hodograph composed of the velocity vectors shown in Fig. 2(a) to 2(e).

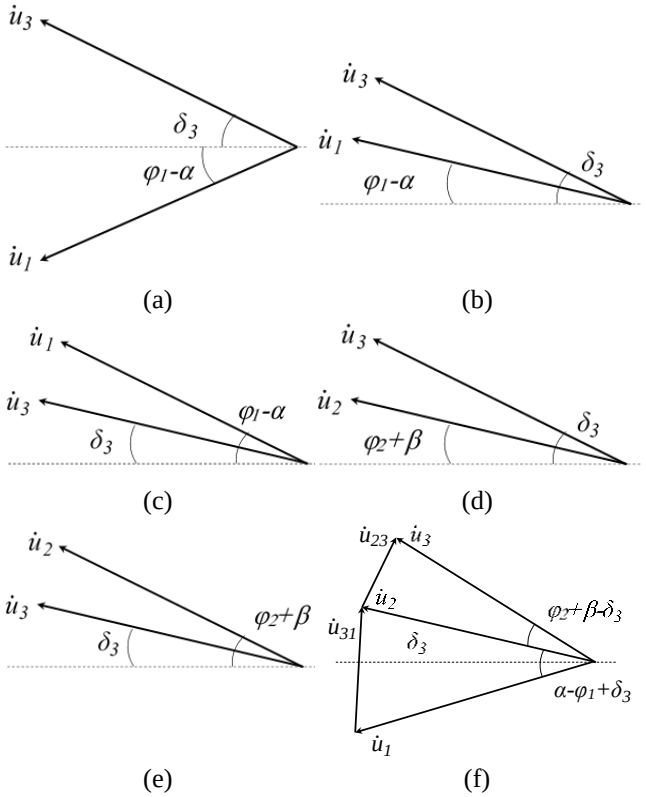

Fig. 2: Velocity vectors compositions: (a)(b)(c) comparison of $\dot{u}_1$and $\dot{u}_3$ alignments, (d)(e) comparison of $\dot{u}_2$and $\dot{u}_3$ alignments (f) an example of velocity hodograph.

Based on the upper bound theorem of limit analysis and according to Eq. (1), since the rate of external work done by surface loads is equal to zero, the rates of internal and external work in the soil wedges of Fig. 2 are as follows:

$$d_1+d_2+d_3+d_{23}+d_{31}\geq(1-k_v)\left[\dot{Z}_1+\dot{Z}_2+\dot{Z}_3\right]+k_h(\dot{Y}_1+\dot{Y}_2+\dot{Y}_3) \quad (2)$$

d_1, d_2 are dissipated energies due to cohesion of backfill and front fill and d_3, d_{23}, and d_{31} are dissipated energies due to adhesion between the wall and the base, the backfill, and the front fill, respectively. Following formulas calculate these parameters:

$$d_1=c_1\dot{u}_1\times(m_3+m_4)\times\cos\phi_1 \quad (3)$$

$$d_2=\frac{c_2\dot{u}_2H_2\cos\phi_2}{\sin\beta} \quad (4)$$

$$d_3=c_3\left(a+H_1\left(\frac{1}{\tan\lambda_1}+\frac{1}{\tan\lambda_2}\right)\right)\dot{u}_3\cos\delta_3 \quad (5)$$

$$d_{13}=\frac{c_{13}H_1\dot{u}_{13}\cos\delta_1}{\sin(\lambda_1)} \quad (6)$$

$$d_{23}=\frac{c_{23}H_2\dot{u}_{23}\cos\delta_2}{\sin\lambda_2} \quad (7)$$

$\dot{Z}_1$, $\dot{Z}_2$and $\dot{Z}_3$, external work rates due to weights of the wedges, are:

$$\dot{Z}_1=W_1\dot{u}_1\sin(\alpha+\phi_1) \quad (8)$$

$$\dot{Z}_2=-W_2\dot{u}_2\sin(\beta+\phi_2) \quad (9)$$

$$\dot{Z}_3=-W_3\dot{u}_3\sin\delta_3 \quad (10)$$

Correspondingly, $\dot{Y}_1$, $\dot{Y}_2$ and $\dot{Y}_3$, external work rates due to inertial forces derived from acting horizontal seismic acceleration, calculated as:

$$\dot{Y}_1=W_1\dot{u}_1\cos(\alpha-\phi_1) \quad (11)$$

$$\dot{Y}_2=W_2\dot{u}_2\cos(\beta+\phi_2) \quad (12)$$

$$\dot{Y}_3=W_3\dot{u}_3\cos\delta_3 \quad (13)$$

W_1, W_2, and W_3 are the weights of the backfill, the front fill, and the wall, respectively. Considering $k_v=Xk_h$ and also assuming that as failure occurs, horizontal seismic coefficient equals yield seismic coefficient ($k_y=k_h$), consequently, external and internal work rates come to be equal:

$$d_1+d_2+d_3+d_{23}+d_{31}=(1-Xk_y)\left[\dot{Z}_1+\dot{Z}_2+\dot{Z}_3\right]+k_y(\dot{Y}_1+\dot{Y}_2+\dot{Y}_3) \quad (14)$$

Q_1, Q_2, Q_{31}, Q_{23} are going to be introduced based on the shape of hodographs to apply conversion of all of the velocity vectors to $\dot{u}_3$. The subscript of Q parameters represents the corresponding vector.

$$\begin{cases} Q_1=\dfrac{\sin(\lambda_1-\delta_3-\delta_1)}{\sin(\alpha+\lambda_1-\phi_1-\delta_1)} & (\delta_3\geq\phi_1-\alpha) \\ Q_1=\dfrac{\sin(\pi-\lambda_1+\delta_3-\delta_1)}{\sin(\pi-\alpha-\lambda_1+\phi_1-\delta_1)} & (\delta_3<\phi_1-\alpha) \end{cases} \quad (15\text{-a})$$

$$\begin{cases} Q_2=\dfrac{\sin(\lambda_2+\delta_3+\delta_2)}{\sin(\lambda_2+\delta_2+\phi_2+\beta)} & (\phi_2+\beta\geq\delta_3) \\ Q_2=\dfrac{\sin(\lambda_2+\delta_3-\delta_2)}{\sin(\lambda_2-\delta_2+\phi_2+\beta)} & (\phi_2+\beta<\delta_3) \end{cases} \quad (15\text{-b})$$

$$\begin{cases} Q_{31}=\dfrac{\sin(\phi_1-\alpha+\delta_3)}{\sin(\alpha+\lambda_1-\phi_1-\delta_1)} & (\delta_3\geq\phi_1-\alpha) \\ Q_{31}=\dfrac{\sin(\phi_1-\alpha-\delta_3)}{\sin(\pi-\alpha-\lambda_1+\phi_1-\delta_1)} & (\delta_3<\phi_1-\alpha) \end{cases} \quad (15\text{-c})$$

$$\begin{cases} Q_{23}=\dfrac{\sin(\beta-\delta_3+\phi_2)}{\sin(\lambda_2+\delta_2+\phi_2+\beta)} & (\phi_2+\beta\geq\delta_3) \\ Q_{23}=\dfrac{\sin(\delta_3-\beta-\phi_2)}{\sin(\lambda_2-\delta_2+\phi_2+\beta)} & (\phi_2+\beta<\delta_3) \end{cases} \quad (15\text{-d})$$

Substituting equations (15) into Eq. (14), k_y calculates as:

$$k_y=\left[\left(Q_1d_1+Q_2d_2+d_3+Q_{23}d_{23}+Q_{31}d_{31}\right)-\left(Q_1\dot{Z}_1+Q_2\dot{Z}_2+\dot{Z}_3\right)\right]/\left[\left(Q_1\dot{Y}_1+Q_2\dot{Y}_2+\dot{Y}_3\right)-X\left(Q_1\dot{Z}_1+Q_2\dot{Z}_2+\dot{Z}_3\right)\right] \quad (16)$$

To obtain the best estimate (the *least* upper bound), the critical yield acceleration coefficient needs to be minimized

with respect to α and β which are the failure angles of back and front fill, respectively. To do so, a computer program in MATLAB environment is developed by the authors. The backbone of this program is based on the optimization procedure developed by Michalowski [17] which uses substitution of various combinations of $5<\alpha,\beta<85$ in Eq. (16) and provides the minimum value for k_y.

Once seismic acceleration takes precedence over yield acceleration $(k>k_y)$, the system begins to slide. In other words, plastic deformations introduce inertial forces due to earthquake acceleration, which must be accounted in Eq. (1). The sliding at the first, the second and the third wedges induces accelerations $\ddot{u}_1$, $\ddot{u}_2$ and $\ddot{u}_3$, respectively. Fig. 3 shows the angle between acceleration vectors and the corresponding failure surface in which ψ is dilation angle ($\psi=0$ for incompressible soil; and $\psi=\varphi$ for an associative soil). The current algorithm can consider $0\le\psi_1\le\varphi_1$, $0\le\psi_2\le\varphi_2$, $0\le\psi_3\le\delta_3$, $0\le\psi_{31}\le\delta_1$ and $0\le\psi_{23}\le\delta_2$. It must be mentioned since wedge acceleration and acceleration vector are in the opposite direction, work rates due to inertial forces are negative. The new energy balance equation is as follows.

$$d_1+d_2+d_3+d_{23}+d_{31}=-m_1\dot{u}_1\ddot{u}_1\cos(\phi_1-\psi_1)-m_2\dot{u}_2\ddot{u}_2\cos(\phi_2-\psi_2)-m_3\dot{u}_3\ddot{u}_3\cos(\delta_3-\psi_3)+(1-Xk)\left[\dot{Z}_1+\dot{Z}_2+\dot{Z}_3\right]+k(\dot{Y}_1+\dot{Y}_2+\dot{Y}_3) \quad (17)$$

In order to convert other acceleration vectors to $\ddot{u}_3$, parameters Q's are introduced, which are exactly similar to Eq. (15), except for the angles φ and δ that are substituted by their corresponding ψ angles of Fig 3.

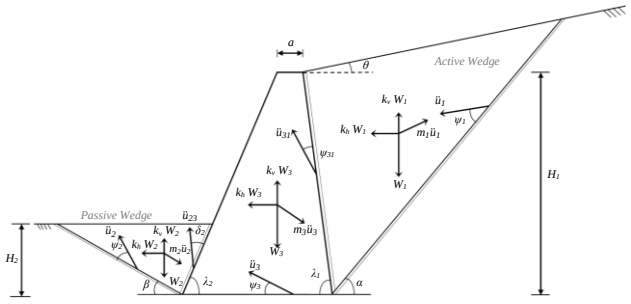

Fig. 3: Displacement mechanism of the gravity retaining wall.

The following equation is a result of replacing equations (14), (15) and (16) with Eq. (18).

$$\ddot{u}_3=(k-k_y)g\left[m_1Q_1\cos(\alpha-\phi_1)+m_3\cos(\delta_3)+m_2Q_2\cos(\phi_2+\beta)-X(\dot{Z}_1+\dot{Z}_2+\dot{Z}_3)\right]/\left[Q_1Q_1'm_1\cos(\phi_1-\psi_1)+Q_2Q_2'm_2\cos(\phi_2-\psi_2)+m_3\cos(\phi_3-\psi_3)\right]=C(k-k_y)g \quad (18)$$

where k is seismic acceleration coefficient and C is the parameter which represents geometrical and mechanical characteristics of the wedges. $\ddot{u}_3$ is a "true" acceleration, and its double time integral results in permanent displacement of the wedge; based on this, double time integration on Eq. (18) yields permanent displacement of the gravity retaining wall.

$$u_3=C\iint g(k-k_y)dtdt \quad (19)$$

The aforementioned formulas are presented for the associative materials and in order to consider nonstandard materials (nonstandard material is the one with deformation governed by the non-associative flow rule) in the formulation, the internal friction angle φ and cohesion c are required to be replaced with following equations [14].

$$\tan\phi^*=\frac{\cos\psi\sin\phi}{1-\sin\psi\sin\phi} \quad (21)$$

$$c^*=c\frac{\cos\psi\cos\phi}{1-\sin\psi\sin\phi} \quad (21)$$

3. Comparison of Equations with Literature

For the wall shown in Fig. 1 with $H_1=8m$, $H_2=0$, $a=0.3m$, $\gamma_1=20$ kN/m3, $\lambda_1=90$, $\lambda_2=60.64$, $\delta_1=0$, $\theta=0$, $W_w=556.8$kN/m where W_w is weight of the wall, α and k_y have been calculated and the results compared to Li et al [18] listed in Table 1.

Table 1. comparison of yield acceleration (k_y) and critical wedge failure angle (α).

		k_y		α	
φ_1	δ_3	Proposed Method	Li et al	Proposed Method	Li et al
25	25	0	0	57.50	57.9
30	30	0.111	0.11	54.67	55.2
35	35	0.224	0.22	52.03	55.0
40	40	0.340	0.34	49.49	49.5

Table 2 is the result of comparison of yield accelerations of a wall with $H_2=0$, $a=0.3m$, $\gamma_1=20$ kN/m^3, $\gamma_3=24$ kN/m^3, $\lambda_1=90$, $\lambda_2=60.642$, $\varphi=30$, $\delta_1=20$, $\delta_3=30$, $c=0$. In this table, L is the width of failure block considered in Hassani's [19] method.

Table 2. comparison of yield acceleration (k_y).

H	Proposed Method	Michalowski [14]	Hassani-Single Block, $L/H=4000$	Hassani-Double Block, $L/H=4000$
3	0.1873	0.181	0.1839	0.181
5	0.1748	0.169	0.1719	0.1694
7	0.1691	0.163	0.1665	0.1644
10	0.1647	0.159	0.1624	0.1606

4. Results and Discussion

In order to have a better understanding of the wall performance and effective parameters, it is assumed all wedges are cohesionless ($c/\gamma H^2=0$). Based on the described algorithm, Fig. 4, shows H_2/H_1 variations with seismic yield coefficient (k_y) for $\varphi_1=\varphi_2=\varphi_3=25,30,35,40$, in which $\delta_1=\delta_2=\delta_3=1/3\varphi,2/3\varphi$. In order to generate the following curves, a wall with $\lambda_1=90$, $\lambda_2=80$, $a=0.0375H_1$, $\gamma_3/\gamma_1=\gamma_3/\gamma_2=1.22$, $\theta=0$ has been considered. It must be noted

that $c/\gamma H^2$ and H_2/H_1 are dimensionless parameters. From the practical point of view, since the influence of the horizontal component of the seismic acceleration is much more in displacement results, the vertical component of the seismic acceleration is assumed to be zero.

Fig. 4 states that increasing the height of the soil in front of a gravity retaining wall results in better performance regarding permanent displacement during an earthquake. It also shows that soils with higher δ values have higher k_y and, simultaneously, by inclination of H_2/H_1 values, it shows a higher rate of growth too.

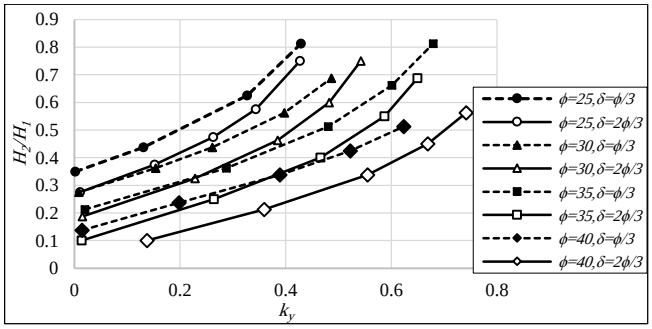

Fig. 4: H_2/H_1 vs k_y for $\delta=1/3\varphi,\ 2/3\varphi$

For a similar wall with $\lambda_1=90,\ \lambda_2=80,\ a=0.0375H_1,\ \gamma_3/\gamma_1=\gamma_3/\gamma_2=1.22,\ \theta=10$, Fig. 5(a) and (b) shows a series of curves for $\varphi_1=\varphi_2=\varphi_3=25,30,35,40$ in which $\delta_1=\delta_2=\delta_3=1/3\varphi,\ 2/3\varphi$. These curves present seismic displacements of the wall against various values of dilation angles (ψ) equal to $0,\varphi/3,\varphi/2,2\varphi/3$ and φ. In order to carry out displacement calculation, friction angles of the soil must be modified using Eq. (20). This modification enables using nonstandard materials in upper bound theorem of limit analysis. The record from earthquake of Bam dating 26/12/2003 has been used to generate the seismic displacement. Table 3 provides information regarding this record.

Table 3. Characteristic of Bam earthquake [17].

Station	Location		Date	PGA	Magnitude		
	Longitude	Latitude	D/M/Y	Cm/s/s	Mw	Ms	Mb
Bam	58.33	29	26/12/2003	989	-	6.7	-

Fig 5 shows that for $\varphi=35$ and $\delta=2\varphi/3$, as dilation angle increases from 0 to φ, displacement declines from 13.43cm to 1.27cm. In other words, since increasing values of ψ generate higher values of k_y, the values of seismic displacement decreases.

The graphs of Fig. 5 state that seismic displacements can vary appreciably depending on internal friction angle. The variation seems less obvious at higher values of friction angle. Generally, inclining values of dilation angle shows declination of seismic displacements.

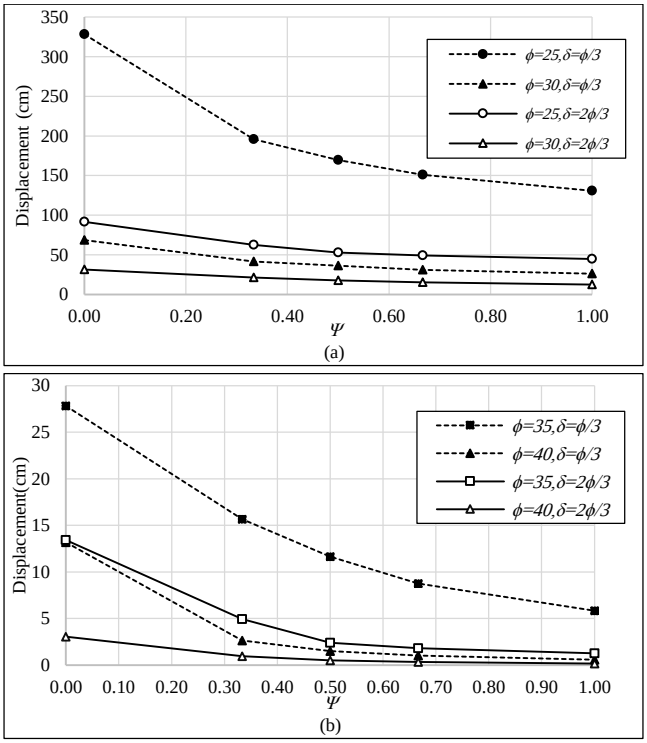

Fig. 5: Seismic Displacement vs dilation angle variations (a) $\varphi=25,\ 30$ (b) $\varphi=35,\ \varphi=40$

5. Conclusion

A series of formulations using upper bound theorem is provided to address displacement of gravity retaining walls under seismic excitation due to sliding. To do so, the strong motions data recorded in Bam is used to undertake Newmark displacement analysis. The provided algorithm takes into account the effect of the soil in front of the wall too. By applying modifications suggested by Michalowski [14], the effect of variation in dilation angle and the height of the front fill to backfill ratio (H_2/H_1) on the results has been investigated. Comparison of H_2/H_1 for different internal frictions designated that greater values of H_2/H_1 give greater values of yield acceleration coefficient which leads to less permanent displacements during an earthquake. Outcomes of seismic displacement versus various dilation angles showed that larger values of $0\le\psi\le\varphi$ lead to smaller seismic displacement, in which the trend is more obvious at $0\le\psi\le\varphi/2$. However, it must be noted, assumptions used for developing algorithm affects their conformity to reality. Thus, these concluded values of k_y and permanent displacement are just propositions, and laboratory tests and more numeric analyses are necessary for verification.

6. Reference

[1] Newmark, N. M. [1965]. "Effects of earthquakes on dams and embankments." Geotechnique 15(2): 139-160.

[2] Richards Jr, R. and D. G. Elms [1979]. "Seismic behavior of gravity retaining walls." Journal of Geotechnical and Geoenvironmental Engineering 105(ASCE 14496).

[3] Nadim, F. and R. V. Whitman [1983]. "Seismically induced movement of retaining walls." Journal of Geotechnical Engineering 109(7): 915-931.

[4] Rafnsson, E. and S. Prakash [1994]. Displacement based aseismic design of retaining walls. Proceedings of The International Conference on Soil Mechanics and Foundation Engineering-International Society for Soil Mechanics and Foundation Engineering, Aa Balkema.

[5] Whitman, R. V. and S. Liao [1985]. Seismic design of gravity retaining walls, Massachusetts Inst of Tech Cambridge Dept Of Civil Engineering.

[6] Deyanova, M., Lai, C. G., & Martinelli, M. [2016]. Displacement–based parametric study on the seismic response of gravity earth-retaining walls. Soil Dynamics and Earthquake Engineering, 80, 210-224.

[7] Taravati, H., & Ardakani, A. [2018]. The numerical study of seismic behavior of gravity retaining wall built near rock face. Earthquakes and Structures, 14(2), 179-186.

[8] Fathipour, H., Siahmazgi, A. S., Payan, M., & Chenari, R. J. (2020). Evaluation of the lateral earth pressure in unsaturated soils with finite element limit analysis using second-order cone programming. Computers and Geotechnics, 125, 103587.

[9] Davis, E. H. [1969]. Theories of plasticity and the failure of soil masses", Ch. 6 of. Soil Mechanics Selected Topics", Ed. IK lee, Butterworth, London.

[10] Chen, W. [1975]. Limit Analysis and Soil Plasticity Elsevier, Science Publishers, Amsterdam.

[11] Michalowski, R., & Mroz, Z. [1978]. Associated and non-associated sliding rules in contact friction problems. Archiwum Mechaniki Stosowanej, 30(3), 259-276.

[12] Drescher, A., & Detournay, E. [1993]. Limit load in translational failure mechanisms for associative and non-associative materials. Géotechnique, 43(3), 443-456.

[13] Veiskarami, M., Kumar, J., & Valikhah, F. (2014). Effect of the flow rule on the bearing capacity of strip foundations on sand by the upper-bound limit analysis and slip lines. International Journal of Geomechanics, 14(3), 04014008.

[14] Michalowski, R. L. [2007]. "Displacements of multiblock geotechnical structures subjected to seismic excitation." Journal of Geotechnical and Geoenvironmental Engineering 133(11): 1432-1439.

[15] Drucker, D., W. Prager and H. Greenberg [1952]. "Extended limit design theorems for continuous media." Quarterly of Applied Mathematics 9(4): 381-389.

[16] Green, R. A. and R. L. Michalowski [2006]. "Shear band formation behind retaining structures subjected to seismic excitation." Foundations of Civil and Environ. Eng 7: 157-69.

[17] Michalowski, R. [1989]. "Three-dimensional analysis of locally loaded slopes." Geotechnique 39(1): 27-38.

[18] Li, X., Y. Wu and S. He [2010]. "Seismic stability analysis of gravity retaining walls." Soil Dynamics and Earthquake Engineering 30(10): 875-878.

[19] Hassani, A. [2016] ‘‘Seismic three-dimensional displacement analysis of retaining walls by limit analysis method,’’ Master thesis, International Institute of Earthquake Engineering and Seismology (IIEES), Tehran, Iran

[20] Miraboutalebi, M., F. Askari and O. Farzaneh [2011]. "Effect of bedrock inclination on seismic slope stability according to Iran seismically data." International Journal of Civil Engineering 9(4): 247-254.

Appendix:

List of Symbols	
k	seismic acceleration coefficient
k_h	horizontal seismic acceleration coefficient
k_v	vertical seismic acceleration coefficient
k_y	yield acceleration coefficient
g	gravity acceleration
φ_1	internal friction angle of backfill
φ_2	internal friction angle of soil at the front of wall
γ_1	unit weight of backfill
γ_2	unit weight of soil at the front of wall
γ_3	unit weight of wall
θ	backfill upper hand angle with horizon
H_1	height of wall and backfill
H_2	height of soil mass at the front of wall
λ_1	wall angle with backfill
λ_2	wall angle with the soil at the front of wall
δ_1	interface friction angles of the wall with backfill
δ_2	interface friction angles of the front soil
δ_3	interface friction angles of the wall with soil at the base
V	volume
S	surface
T_i	external work rate of surface load
υ_i	deformation velocity
X_i	external work rate of distributed forces
υ_i^k	kinematically admissible velocity field
σ_{ij}	associated stress field
$\dot{\varepsilon}_{ij}$	strain rate
$\dot{u}_1$	velocity of back wedge
$\dot{u}_2$	velocity of front wedge
$\dot{u}_3$	velocity of wall
$\dot{u}_{31}$	relative velocity between wall and back wedge
$\dot{u}_{23}$	relative velocity between wall and front wedge
d_1	dissipated energy due to cohesion of backfill
d_2	dissipated energy due to cohesion of front fill

d_3 dissipated energy due to adhesion between the wall and the base

d_{23} dissipated energy due to adhesion between the wall and backfill

d_{31} dissipated energy due to adhesion between the wall front fill

$\dot{Z}_1$ external work rate due to weights of the back wedge

$\dot{Z}_2$ external work rate due to weights of the back wedge

$\dot{Z}_3$ external work rate due to weights of the wall

$\dot{Y}_1$ external work rate of back wedge due to inertial forces derived from acting horizontal seismic acceleration

$\dot{Y}_2$ external work rate of front wedge due to inertial forces derived from acting horizontal seismic acceleration

$\dot{Y}_3$ external work rate of wall due to inertial forces derived from acting horizontal seismic acceleration

W_1 weight of back-soil wedge

W_3 *and* W_w weight of wall

W_2 weight of front-soil wedge

W a general parameter for weight of wedges

Q_1 coefficient applied to velocity vector $\dot{u}_1$ to be converted to $\dot{u}_3$

Q_2 coefficient applied to velocity vector $\dot{u}_2$ to be converted to $\dot{u}_3$

Q_{23} coefficient applied to velocity vector $\dot{u}_{23}$ to be converted to $\dot{u}_3$

Q_{31} coefficient applied to velocity vector $\dot{u}_{31}$ to be converted to $\dot{u}_3$

α critical angle of back wedge

β critical angle of front wedge

$\ddot{u}_1$ acceleration of back wedge

$\ddot{u}_2$ acceleration of front-soil wedge

$\ddot{u}_3$ acceleration of wall

$\ddot{u}_{31}$ relative acceleration between the front wedge and the wall

$\ddot{u}_{23}$ relative acceleration between the back wedge and the wall

Ψ_1 dilation angle of back wedge

Ψ_2 dilation angle of front wedge

Ψ_3 dilation angle of wall

Ψ_{31} dilation angle between the front wedge and the wall

Ψ_{23} dilation angle between the back wedge and the wall

C a parameter represents geometrical and mechanical characteristics of the wedges

ϕ^* corrected ϕ for non-standard materials

c^* corrected c for non-standard materials